© 2022 IEEE. Personal use of this material is permitted. Permission from IEEE must be obtained for all other uses, in any current or future media, including reprinting/republishing this material for advertising or promotional purposes, creating new collective works, for resale or redistribution to servers or lists, or reuse of any copyrighted component of this work in other works.

ANALYSIS OF NEAR-FIELD PROBING TECHNIQUES FOR IMMUNITY TESTS

Xinglong Wu(1), Flavia Grassi (1), Giordano Spadacini (1) , Sergio A. Pignari (1), Umberto Paoletti (2), Isao Hoda (2)

(1) Dept. Electronics, Information and Bioengineering, Politecnico di Milano,
Piazza L. da Vinci, 32, 20133, Milan, Italy., Email: {xinglong.wu; flavia.grassi, giordano.spadacini, sergio.pignari}@polimi.it
(2) Center for Technology Innovation – Production Engineering, Research & Development Group, Hitachi Ltd,
Yokohama 244-0817, Japan. Email: {umberto.paoletti.ff, isao.hoda.tb}@hitachi.com

ABSTRACT

This work experimentally investigates the performance of near-field probes as injection devices for wideband immunity tests. To this end, the coupling effectiveness and resolution of different kinds of magnetic and electric near-field probes are firstly investigated in terms of *S*-parameters measured with the probes placed on microstrip traces. Different test benches are set up and experimentally characterized in order to investigate the characteristics and determine the frequency response of the transfer function of a typical measurement chain for immunity verification. Finally, time-domain near-field tests employing arbitrary waveform generators are introduced, showing the feasibility of injecting customized wideband noise waveforms at specific pins.

1. INTRODUCTION

Electromagnetic compatibility (EMC) issues attract increasing attention in the aerospace industry due to the continued demand for higher integration and reliability of electronic systems in air and space vehicles. A proper EMC design at the early design stages is not only of great importance but also very challenging. Traditional radiated susceptibility tests allow for an overview of the immunity performance of the device under test (DUT). However, the usually large DUT complexity makes it difficult to find the correlation between immunity failures and specific design weaknesses or noise propagation paths. Furthermore, since traditional EMC tests are usually carried out at the end stage of the design process, modifications are expensive and time-consuming.

To provide the designer with a suitable tool to identify possible immunity issues in product prototypes before the design is finalized, a possible solution is to resort to the use of near-field probes. This technique, originally introduced for near-field measurement [1], [2] and emission source modelling [3]-[5], more recently has been extended also to electromagnetic susceptibility analysis [6], [7] where near-field probes are used as injection devices rather than measurement tools. Compared with traditional radiated susceptibility tests or direct radiofrequency power injection method [8], near-field tests not only are available for module- and PCB-level testing but can also provide detailed information on weak components and/or noise propagation paths [9]-[12]. Indeed, near-field probes can be used to detect EM-sensitive areas at IC [6], [13] and PCB [14], [15] levels. Furthermore, by properly placing probes on IC pins/nets, one can evaluate the EM-immunity performance of specific electronic components [15], [16]. Therefore, it is of great importance to investigate the performance of different near-field probes and the corresponding test setups to ascertain their suitability for immunity analysis.

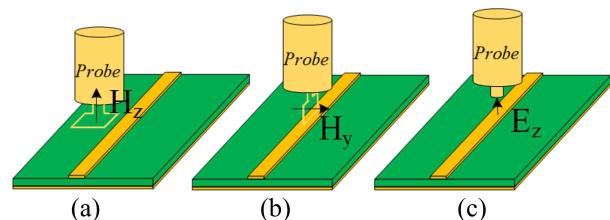

Figure. 1. Principle drawing of near-field probes to measure the (a) orthogonal H-field, (b) tangential H-field, (c) orthogonal E-field from a PCB trace.

For the aforesaid reasons, this work presents an experimental investigation of the performance of near-field probes, in view of their exploitation for immunity testing. To this end, the near-field coupling performance of different probes is investigated. Both magnetic and electric near-field probes are considered, and their coupling effectiveness and resolution are evaluated by S-parameter Vector Network Analyzer (VNA) measurements. Then, different test benches are set up to investigate possible practical issues in near-field immunity tests. A time-domain test involving arbitrary waveform generators and power amplifiers is finally carried out, showing the possibility to predict and inject the desired wideband stress waveforms at the input pins of the IC under test.

2. MAGNETIC AND ELECTRIC NEAR-FIELD PROBES

There is a wide variety of near-field probes, whose design is optimized to selectively measure a specific component of the electric and magnetic field generated by the noise propagating along a PCB trace. Three explicative examples are shown in Fig. 1. A brief theoretical discussion about those probes for electrostatic discharge tests can be found in [14]. The probe in Fig. 1(a) is designed to measure the orthogonal magnetic field perpendicular to the PCB plane, which is especially

useful when there exists a small current loop on a PCB surface. The Langer RF B 3-2, which belongs to this class, will be used in this investigation, and is hereafter referred to as "H_z probe". The probe in Fig. 1(b) is used to detect the orthogonal magnetic field which is parallel to the PCB plane. A customized probe with a small vertical loop at the tip will be considered as an example and will be referred to as "H_y probe". Fig. 1(c) shows a probe for measuring the orthogonal electric field from a PCB trace. Here, the RG405 probe introduced in [15], which is a hand-made probe realized by means of a coaxial cable RG405 with 1 mm bare tip, will be used and referred to as "E_z probe", for short.

3. COUPLING PERFORMANCE

The coupling effectiveness is an essential parameter to characterize the performance of a near-field probe either used as a measurement tool or as an injection device. To investigate and compare the coupling performance of the near-field probes previously introduced, *ad hoc* PCBs are designed. The probes are placed on a PCB microstrip trace (with solder mask), and the transmission coefficient from the probe input to the output terminals of the trace are measured by a VNA Keysight E5071C. Measurements inherently include the effects introduced by the PCB trace and the probe. Conversely, propagation effects along VNA cables are excluded through calibration (calibration kit Agilent N4431B). Details on the impact of the PCB traces (including probe-to-trace coupling) can be found in [15] and [10], respectively. The influence of different types of probes on coupling effectiveness will be addressed in the following sub-sections.

3.1. Preliminary test with the H_z probe

Probe positioning assuring the highest coupling should be identified as the first step of the analysis. Indeed, it is straightforward that placing the H_y and E_z probes directly on the trace under test yields maximum coupling. This is no longer true for the H_z probe since the main magnetic field on the trace surface is the tangential one. Hence, for this probe the maximum coupling is achieved by placing the H_z probe not on top but by the side of the trace under analysis.

For this reason, a preliminary test with the H_z probe (see: Fig. 2(a)) is carried out in order to identify its best positioning. For the experiment, a 149 mm long microstrip line printed on the top layer of the fabricated PCB and covered by a 0.03 mm thick FR4-based solder mask is considered. The nominal trace width and thickness are 0.15 mm and 35 µm, respectively. The nominal thickness of the FR4 substrate (relative permittivity of 4.7 and loss tangent of 0.014) is 80 µm. The S-parameters of the setup were firstly measured with the probe on top of the trace, i.e., "Central" position in Fig. 2(b), and then by moving the probe in different

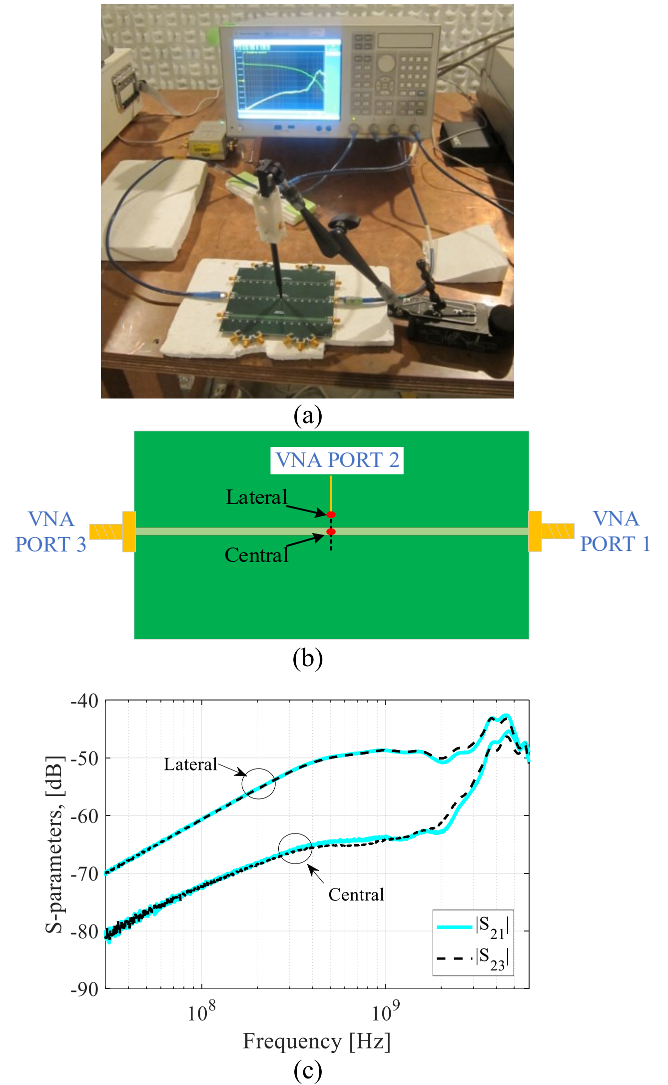

Figure. 2. Experimental investigation of the probe positions for H_z probe: (a) Test setup, (b) Top-view of the test setup, (c) Measurement results.

positions along the vertical black dash line in Fig. 2(b), i.e., "Lateral" position. The obtained transmission coefficients are compared in Fig. 2(c). It is clearly shown that if the H_z probe is placed on a proper lateral position close to the trace, the coupling effectiveness significantly increases with respect to the case in which it is placed on top of the trace. Namely, the corresponding transmission coefficient (see curves labelled as "Lateral") is around 10 dB higher than the one obtained for the "Central" position up to 2 GHz. Such a difference progressively decreases while the frequency increases. Above 5 GHz, the two positions yield comparable coupling.

3.2. Investigation of coupling effectiveness and spatial resolutions

In this sub-section, the coupling effectiveness and spatial resolution of the near-field probes under analysis are investigated. To this end, a PCB involving three parallel

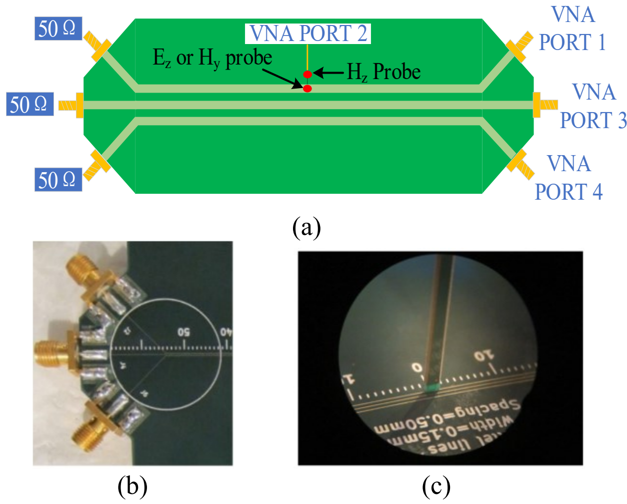

Figure. 3. Test setup for experimental investigation of the probe coupling performance: (a) Principle drawing, (b) Specific arrangement of the terminal sections of the PCB, (c) Positioning of the H_y probe.

traces (see: Fig. 3(a)) was fabricated and considered as the PCB under test. In this PCB, the length of the traces, and their edge-to-edge separation are 134 mm and 0.15 mm, respectively. A specific terminal arrangement was proposed (see: Fig. 3(b)) in order to allow soldering SMA connectors, yet maintaining the same length for all traces. Other geometrical and electric parameters of this PCB are the same as the one introduced in Sec. 3.1. As shown in Fig. 3(a), measurements were carried out with the E_z and H_y probes placed on top (at midpoint) of one of the outer traces (see Fig. 3(c) for the positioning of the H_y probe). Conversely, the H_z probe was placed by the side of the trace (midpoint) according to the analysis presented in Sec. 3.1.

The obtained measurement results are depicted in Fig. 4. The S-parameters S_{21}, S_{23} and S_{24} represent the coupling coefficient between (a) the probe and the outer trace under test (S_{21}), (b) between the probe and the inner nearby trace (S_{23}), and between the probe and the outer trace on the other side (S_{24}). The second and third coefficients provide information to quantify spatial resolution / crosstalk. Fig. 4(a) indicates that with respect to the H_z probe, the H_y probe assures higher coupling in the low frequency range (< 500 MHz) but lower coupling at high frequency. The E_z probe shows the highest coupling performance. This is mainly due to the fact that among the three probes, the E_z one has the thinnest dielectric separation between the probe tip and the copper trace. Indeed, the tip of the E_z probe is bare. Hence, the PCB solder mask represents the only insulation. Conversely, the tips of the H_z and H_y probes (see: Fig. 3(c)) are covered by dielectric material, which assures electric insulation in case of bare traces (like IC pins) but generally increases the distance between the tip and the trace under test. The phase information of the S_{21} is shown in Fig. 4 (b). This frequency behavior is in line

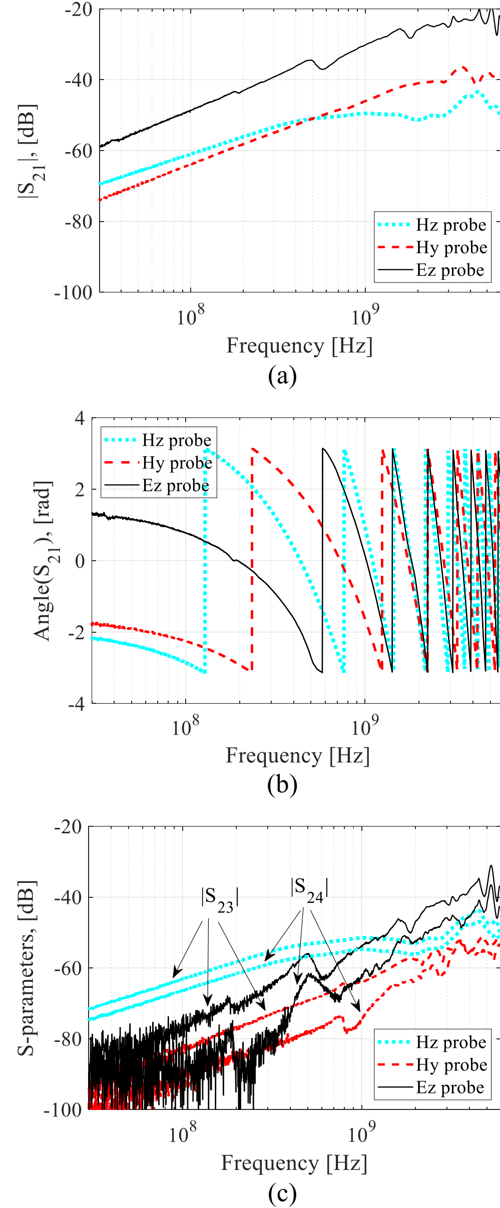

Figure. 4. Experimental investigation of coupling performance: (a) Coupling effectiveness (Magnitude), (b)Coupling effectiveness (Phase) (c) Spatial resolution.

with transmission line theory, which is consistent with the fact that both the PCB trace and the probe behave as transmission-line structures.

From Fig. 4(c) it can be observed that the H_y probe exhibits the lowest coupling with nearby traces. The E_z probe has higher coupling than the H_y one especially in the high frequency range. The H_z probe shows the worst performance in terms of spatial resolution. This can be clearly appreciated by comparing the plots in Fig. 4(a) and Fig. 4(c). Indeed, the magnitudes of the transmission coefficients S_{23} and S_{24} for the H_z probe are not only higher than those of the other probes, but just slightly smaller than the corresponding S_{21} parameter. This is

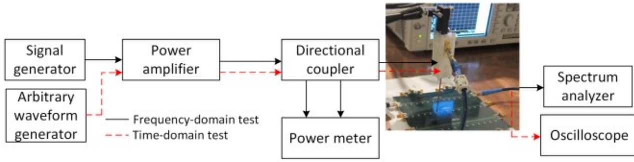

Figure. 5. Principle drawing of the immunity test setup involving near-field probes.

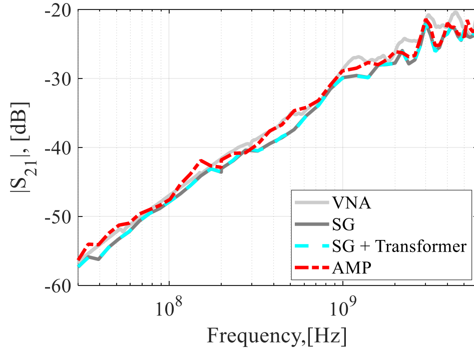

Figure. 6. Frequency-domain measurement results.

probably due to the fact that the other two nearby traces significantly affect the distributions of the H-field loop. Based on the above results and discussion, the E_z probe is selected and hereafter considered in the reminder of this work.

4. TRANSFER FUNCTION OF THE MEASUREMENT CHAIN

To investigate practical issues possibly encountered during the test (such as instruments' grounding), the coupling coefficients measured by resorting to the VNA are preliminary compared with those obtained in traditional immunity setups involving a signal generator (SG) and power amplifiers (AMPs) (see solid black lines in Fig. 5). In these setups, the E_z probe was mounted on the middle of the PCB trace in Sec. 3.1. Starting from the obtained measurement data, the magnitude of the transmission coefficient S_{21} is evaluated as

$$S_{21_{SG}} = P_{SA} - P_{SG} + |S_{cp}| - G_{AMP} \quad (1)$$

where P_{SA} (in dBm) is the input power of the spectrum analyzer, P_{SG} (in dBm) is the output power of the signal generator, S_{cp} (in dB) is the transmission coefficient of the directional coupler, and G_{AMP} (in dB) is the amplification factor of the AMPs.

The test results are shown in Fig. 6. "VNA", "SG" and "SG+AMP" indicate the test setups involving VNA, SG and both SG and AMPs, respectively. In the test setup labelled as "SG + transformer", an additional insulation transformer was added to the "SG" setup between the spectrum analyzer and the plug, so to manually separate its ground from the one of the SG. The good agreement shown in Fig. 6 proves the effectiveness and significance of the S-parameter characterization previously carried out also in combination with traditional instrumentation for immunity verification.

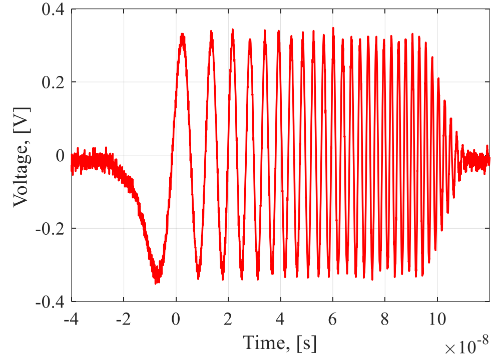

(a)

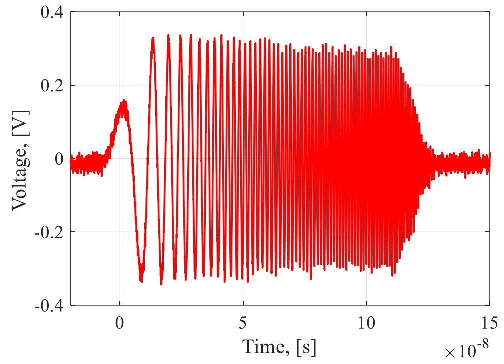

(b)

Figure. 7. Measured signals generated by the AWG: (a) 30 MHz – 400 MHz and (b) 80 MHz – 1000 MHz. It is worth mentioning that these signals and output signals are not measured simultaneously.

5. TIME-DOMAIN IMMUNITY TEST

For testing robustness of electronic devices, it is often of interest to assess the immunity of components to impulsive stress waveforms, that is to directly run the test in the time domain. In this case, it is expected that the shape of the wideband noise waveform to be injected is distorted due to noise propagation along the measurement chain [12]. Therefore, the actual shape of the waveform at the pin of IC under test (referred as to "V_{out}") may significantly differ from the waveform generated by the generator (an arbitrary waveform generator (AWG) is required in this case). In order to predict the actual voltage induced at the output, i.e., voltage V_{out}, the transfer function of the whole measurement chain should be preliminary characterized.

Thanks to the results preliminary obtained in Sec. 4, the transfer function of the measurement chain can be obtained by combining the S-parameters measured at the ports of each component. Both VNA measurements, or full-wave simulations or circuit-models can be used to this purpose.

The test setup is presented in Fig. 5 (see dashed red lines). The S-parameters of the coupling area including the probe and PCB traces were obtained by full wave simulations, whereas the S-parameters of all other parts were retrieved by VNA measurements. By combining the measured waveform generated by the AWG (input voltage, shown in Fig. 7) and the S-parameters associated with the measurement chain (including the coupling area), the output waveforms can be predicted. Specifically, the S-parameters of the measurement chain (i.e., the amplification system, the probe, the PCB and the output cables) are modelled in Keysight ADS circuit simulator (see: Fig. 8), in order to obtain the transfer function from the AWG to the oscilloscope required to predict the output waveforms (given specific input waveforms generated by the AWG). It is worth mentioning that although here 50 Ω terminations are considered, the proposed procedure is general, and can be applied also for different terminal conditions.

During the test, two chirps (30 MHz – 400 MHz and 80 MHz – 1000 MHz, see Fig. 7) were generated by the AWG and injected into the system. Fig. 9(a) and (b) present the measured and predicted output waveforms, showing a satisfactory agreement, and confirming the feasibility of the proposed approach.

6. NEAR-FIELD IMMUNITY TESTS VS TRADITIONAL SUSCEPTIBILITY TESTS

Traditional radiated/conducted susceptibility procedures are unit/system-level tests aimed at assessing the immunity of unit/sub-systems to external interference. In this perspective, it is not possible to strictly correlate traditional susceptibility tests to the proposed near-field procedure, whose main objective is to provide PCB designers with a diagnostic tool to investigate the intra-system compatibility between internal components, as well as to identify susceptible components at PCB level. Pertinent test levels and stress waveforms should be determined by considering the internal noise sources, and can be different depending on the specific applications. Establishing a strict correlation between the proposed near-field procedure and traditional RS/CS tests is anyway possible. To this end, proper level and stress waveforms to be injected by near-field tests can be obtained by preliminary simulation and/or measurement of the system under test (i.e., including cables, enclosure, and PCBs), for instance, by following an approach similar to the one presented in [17].

7. CONCLUSION

This work discussed several issues related to the possible use of near-field probes as injection devices for wideband immunity tests. Three kinds of near-field probes where compared in terms of coupling performance through an experimental investigation in the frequency range 30 MHz - 6 GHz. The analysis has proved that the electric

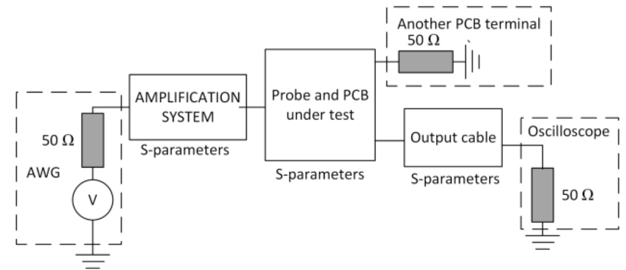

Figure. 8. Principle drawing of the whole injection system.

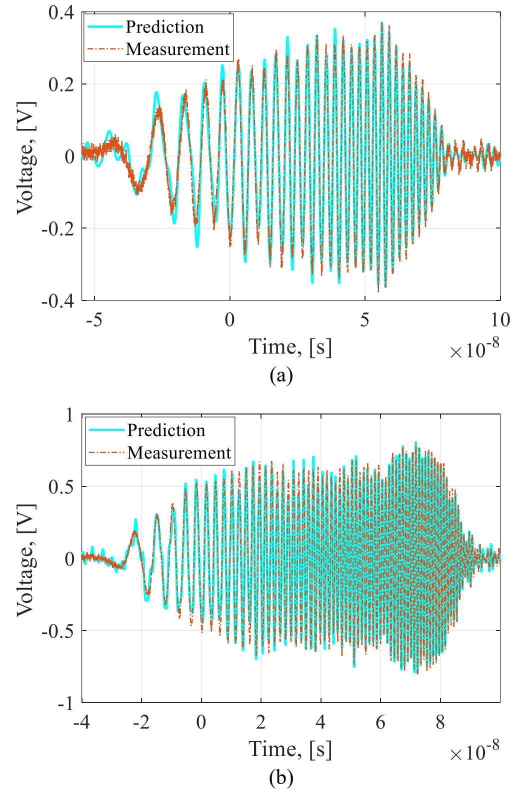

Figure. 9. Predicted and measured time-domain waveform Vout with injected chirps set in the frequency range (a) 30 MHz – 400 MHz and (b) 80 MHz – 1000 MHz.

near-filed probe with bare tip assures higher coupling, since the distance between the probe tip and the trace under test is minimized (i.e., it is only due to the PCB solder mask). However, at high-frequency (> 2 GHz) such a probe can introduce higher noise levels on nearby traces. The frequency-domain tests experimentally prove the equivalence between the VNA and SG-AMP system measurements, even in the case with different grounding strategies of the instruments. The time-domain tests show the feasibility of injecting customized wideband noises by using a traditionally immunity test system.

These results confirm that the use of near-field probes for intra-system immunity verification at component and PCB levels looks promising. However, in a unit level EMC test, the actual stress noise level and shape injected

into the component under test is dependent on internal excitation interactions in the unit. Therefore, further investigations are required to bring out a database of typical noise sources in the aerospace devices to avoid the risk of overtesting or undertesting components.

8. REFERENCES

1. Y. Gao & I. Wolff (1998), Miniature electric near-field probes for measuring 3-D fields in planar microwave circuits, IEEE Trans. Microw. Theory Techn., vol. 46, no. 7, pp. 907–913.

2. D. Baudry, C. Arcambal, A. Louis, B. Mazari, & P. Eudeline (2007), Applications of the near-field techniques in EMC investigations, IEEE Trans. Electromagn. Compat., vol. 49, no. 4, pp. 805–815.

3. J. Shi, M. A. Cracraft, J. Zhang, R. E. DuBroff & K. Slattery (2004), Using near-field scanning to predict radiated fields, in *Proc. Int. Symp. Electromagn. Compat.,* Silicon Valley, USA, pp. 14-18.

4. X. Tong, D. W. P. Thomas, A. Nothofer, P. Sewell, & C. Christopoulos (2010), Modeling Electromagnetic Emissions from Printed Circuit Boards in Closed Environments Using Equivalent Dipoles IEEE Trans. Electromagn. Compat., vol. 52, no. 3, pp 462-470.

5. Y. Zhao et al. (2020), Measurement of Near-Field Electromagnetic Emissions and Characterization Based on Equivalent Dipole Model in Time-Domain, IEEE Trans. Electromagn. Compat., vol. 62, no. 4, pp. 1237-1246.

6. A. Boyer, S. Benhia, & E. Sicard (2007), Characterization of electromagnetic susceptibility of integrated circuits using near-field scan, Electron. Lett., vol. 43, no. 1.

7. D. Pommerenke, G. Muchaidze, J. Koo, Q. Cai, & J. Min (2007), Application and limits of IC and PCB scanning methods for immunity analysis, in Proc. 18th Int. Zurich Symp. Electromagn. Compat., pp. 83–86.

8. Integrated Circuits—Measurement of Electromagnetic Immunity—Part 4: Direct RF Power Injection Method, IEC Standard 62132-4, 2006.

9. Dubois et al. (2008), Near-field electromagnetic characterization and perturbation of logic circuits, IEEE Trans. Instrum. Meas., vol. 57, no. 11, pp. 2398–2404.

10. X. Wu, F. Grassi, S. A. Pignari, U. Paoletti & I. Hoda (2020), Performance of Electric Near-Field Probes for Immunity Tests, in Proc. XXXIII General Assembly Sci. Symp. Int. Union Radio Sci., (URSI GASS), Rome, Italy, pp. 1-4.

11. S A. Durier, S. Ben Dhia & T. Dubois (2019), Development and validation of a wide band Near Field Scan probe for the investigation of the radiated immunity of Printed Circuit Boards, in Proc. Joint Int. Symp. Electromagn, Compat. and Asia-Pacific Int. Symp. Electromagn. Compat., Sapporo, Japan, pp. 649-652.

12. X. Wu, F. Grassi, G. Spadacini, S. A. Pignari, U. Paoletti & I. Hoda, Test design methodology for time-domain immunity investigations using electric near-field probes, IEEE Trans. Electromagn. Compat., Early Access, DOI: 10.1109/TEMC.2022.3149537

13. A. Boyer, B. Vrignon, J. Shepherd, & M. Cavarroc (2014), Evaluation of the near-field injection method at integrated circuit level, in Proc. Int. Symp. Electromagn. Compat., Goteborg, Sweden, pp. 85–90.

14. G. Muchaidze, et al.(2008), Susceptibility scanning as a failure analysis tool for system-level electrostatic discharge (ESD) problems, IEEE Trans. Electromagn. Compat., vol. 50, no. 2, pp. 268–276.

15. X. Wu, F. Grassi, G. Spadacini, S. A. Pignari, U. Paoletti & I. Hoda (2020), Investigation of Semi-Rigid Coaxial Test Probes as RF Injection Devices for Immunity Tests at PCB Level, IEEE Access, vol. 8, pp. 147919-147929.

16. M. Girard, T. Dubois, G. Duchamp, & P. Hoffmann (2016), EMC susceptibility characterization of an operational amplifier-based circuit combining different technique, in Proc. Int. Symp. Electromagn. Compat. EMC-EUROPE, Wroclaw, Poland, pp. 300–305.

17. Frazier, S., & Sebacher, K. (1994). Development of a bulk current injection direct-drive system to test system level components with stress waveforms that are encountered during full threat indirect effects lightning. NAVAL AIR WARFARE CENTER AIRCRAFT DIV PATUXENT RIVER MD.